Composites Part B 182 (2020) 107613

Contents lists available at ScienceDirect

Composites Part B

journal homepage: www.elsevier.com/locate/compositesb

Highly effective electromagnetic wave absorbing Prismatic Co/C nanocomposites derived from cubic metal-organic framework

Jie Li, Peng Miao, Kai-Jie Chen **, Jian-wei Cao, Jin Liang, Yusheng Tang, Jie Kong *

MOE Key Laboratory of Materials Physics and Chemistry in Extraordinary Conditions, Shaanxi Key Laboratory of Macromolecular Science and Technology, School of Science, Northwestern Polytechnical University, Xi'an, 710072, PR China

ARTICLE INFO

Keywords:
Electromagnetic wave absorption
Co/C nanocomposites
Metal-organic framework

ABSTRACT

In this contribution, the cubic metal-organic framework of $[Co(INA)_2]$ was designed and synthesized by using a cheap and non-toxic ligand of isonicotinic acid (INA). After pyrolysis at 600–700 °C in argon atmosphere, the prismatic Co/C nanocomposites were obtained with cobalt nanoparticles in graphitic carbons. The nanocomposites show favorable impedance matching and extraordinary electromagnetic wave absorption performance from C band to Ku band. The Co/C-650 pyrolyzed at 650 °C shows the best electromagnetic wave absorption at a thickness of 2.0 mm, i.e. a minimum reflection coefficient of −47.6 dB and a broad effective absorption bandwidth of 5.11 GHz. The novel prismatic Co/C nanocomposites possess great potential in smart electromagnetic wave absorbing/shielding devices and systems.

1. Introduction

Electromagnetic (EM) wave radiation and pollution threaten environment and human's life as the rapid development of electronic devices and equipments [1–3]. To solve this problem, numerous EM wave absorbers or shielding materials were developed with low planar density, thinner feature and highly effective absorbing performance, such as broad effective absorption bandwidth (EAB) and low reflection coefficient (RC) [4–6]. The popular and well-accepted EM wave absorbing materials are classified into ferrites, metal alloys, electronic conductive polymers or carbon materials, dielectronic materials, metamaterials, etc. Ferrites and metal alloys usually show strong EM wave absorption at a low frequency of 2–8 GHz [7,8], however, their low EAB, high density, large thickness and weak anti-oxidation properties restrained their application in electronic devices and equipments. Carbon-based composites received great attention due to high electrical conductivity, lower density, high thermal stability and good corrosion resistance [9–12], such as carbon nanotube [13,14], porous carbon [15,16], and graphenes [17,18]. However, such materials always possess high permittivity and low permeability, resulting in impedance mismatch and low EM wave absorption efficiency. It is well known that the attenuation of EM wave in media is mainly attributed to magnetic loss and dielectric loss. Magnetic loss contains domain wall resonance eddy current effect, magnetic domain resonance and ferromagnetic resonance. Dielectric loss mainly includes polarization and conductive loss. The impedance matching is a vital factor to EM wave absorption. Although those materials based on magnetic loss and dielectric loss exhibited good EM microwave absorption in some degree, the individual disadvantage mentioned above limit their wide application. It is still a noticeable challenge to develop new highly efficient EM wave absorbing materials especially via a convenient and efficient strategy.

Metal-organic framework (MOF) is a kind of three- or two-dimensional skeletons consisting of tunable metal atoms/clusters and organic ligands. The existence of metal and organic components make it possible for preparation of hybrid or inorganic materials via pyrolysis, which possesses great potential in highly efficient EM wave absorbers. The carbon-based nanocomposites derived from MOFs have received attention in recent years. The in situ formed magnetic metal or metal oxide clusters or nanoparticles extensively can tune magnetic loss and dielectric loss. It is beneficial to the impedance match and EM wave absorption. Thus the uniform dispersion of magnetic clusters or nanoparticles greatly promoted the multiple reflection loss of EM waves in absorbers [19]. Cobalt-based MOFs are usually selected due to the inherent strong saturation magnetization and high Curie temperature [20]. Che's group prepared Co@NC@RGO from Co-MOF@GO, the optimized minimum RC is −46.5 dB and the EAB is 9.4 GHz at a

* Corresponding author.
** Corresponding author.
E-mail addresses: ckjiscon@nwpu.edu.cn (K.-J. Chen), kongjie@nwpu.edu.cn (J. Kong).

https://doi.org/10.1016/j.compositesb.2019.107613
Received 21 September 2019; Received in revised form 19 November 2019; Accepted 19 November 2019
Available online 27 November 2019

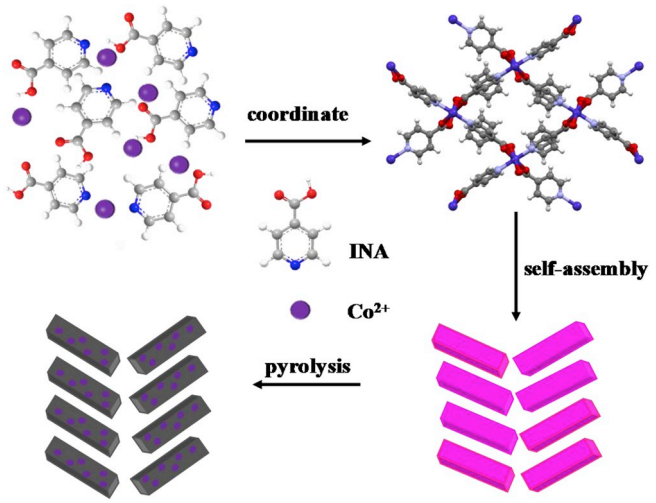

Fig. 1. Schematic illustration of the synthesis of cubic MOF[$Co(INA)_2$] by using a cheap and non-toxic ligand of isonicotinic acid (INA) and in-situ formation of prismatic Co/C nanocomposite via pyrolysis process.

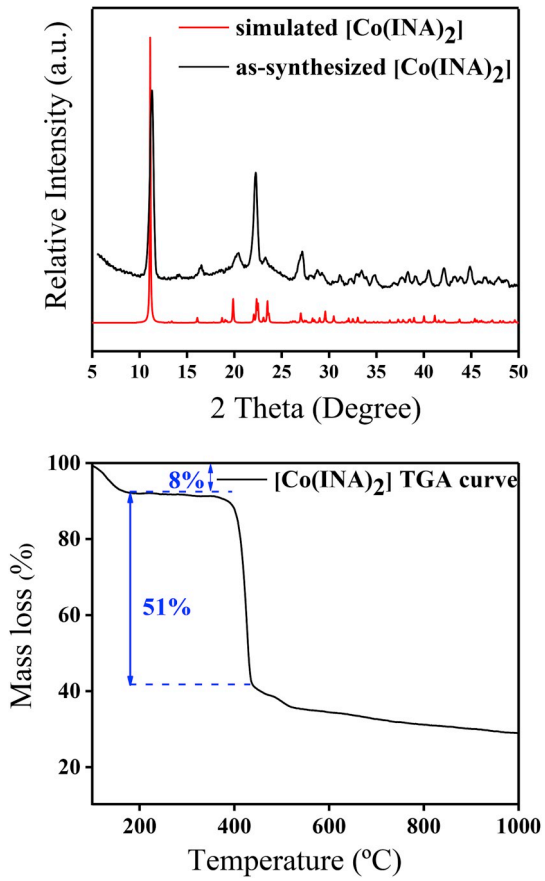

Fig. 2. Theoretical and experimental XRD patterns of cubic [$Co(INA)_2$] MOF and TGA curve of [$Co(INA)_2$] MOF under argon atmosphere.

thickness of 3.5 mm [21]. Shu et al. fabricated Co–C/MWCNTS derived from Co/Zn-MOFs, the minimum RC can achieve −50 dB when the thickness is only 2.4 mm. At the same time, the EAB can cover almost the whole X band of EM wave [22]. Our group carbonized the zeolitic imidazolate frameworks (ZIF) wrapped with poly(dimethylsilylene) diacetylenes. The dielectric loss and magnetic loss can be simultaneously tuned in this heterostructured nanocomplex. Its RC of EM wave

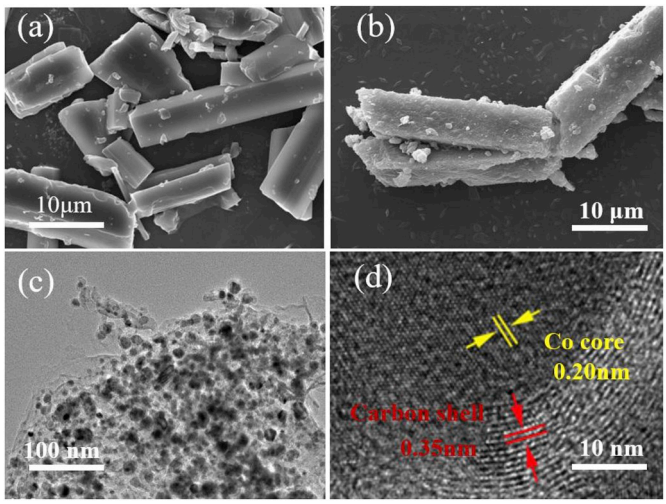

Fig. 3. SEM graphs of cubic [$Co(INA)_2$] MOF(a), prismatic Co/C-650 nanocomposite (b), TEM image with a high resolution of Co/C-650 nanocomposite (c and d).

can reach −50.9 dB at a thickness of 1.9 mm and EAB can cover the whole Ku band (12.0 GHz–18.0 GHz) [23]. The Co-based MOF (CPT-1-Co) from $Co(OAC)_2$ salt and multidentate ligand was obtained to prepare porous Co/C nanocomposites with RC of 5.4 GHz at a thickness of only 1.4 mm [24].

Although various Co/C nanocomposites derived from MOFs were well studied, their high cost and toxicity of organic ligands, such as dimethylimidazole and multidentate ligands, limited their wide application in EM wave absorbers or shielding materials. The Co/C nanocomposites. From a composites engineering viewpoint, the Co/C nanocomposites are generally used in EM wave absorbing or shielding coating, waves or three-dimensional structures. The mass products are always necessary. So the exploration of convenient and highly efficient strategy for Co-containing MOF and Co/C nanocomposites is very important in this field. The isonicotinic acid (INA) is cheap and non-toxic, which can be easily obtained from industrial production. In this work, we synthesized cubic MOF ([$Co(INA)_2$]) from INA and cobalt salt by an eco-friendly and convenient method. Then the [$Co(INA)_2$] MOF was employed to prepare prismatic Co/C nanocomposites by pyrolyzed at 600–700 °C. The prismatic nanocomposites show favorable impedance matching and extraordinary EM wave absorption efficiency in a wide electromagnetic wave frequency from C to Ku band of EM wave.

2. Experiment section

2.1. Materials

Cobalt nitrate hexahydrate ($Co(NO_3)_2{\cdot}6H_2O$, 99.99%, metals basis) and isonicotinic acid (INA, 99%, analytically pur) were purchased from Macklin in Shanghai, China. All the reagents and solvents were used without any purification.

2.2. Synthesis of cubic Co-based MOF ([$Co(INA)_2$])

The preparation method of MOF is described as follows [25]. First, 0.123 g $Co(NO_3)_2{\cdot}6H_2O$ and 0.103 g INA were dissolved in 30 mL ethanol, stirred until completely dissolution. Then the mixture was transferred into 50 mL hydrothermal reactor (auto Teflon-lined autoclave) for reaction at 100 °C for 24 h. After cooling to room temperature, the mixture was taken out to remove the supernatant, washed with alcohol for three times. The pink crystal was obtained after drying in vacuum at 60 °C for 24 h.

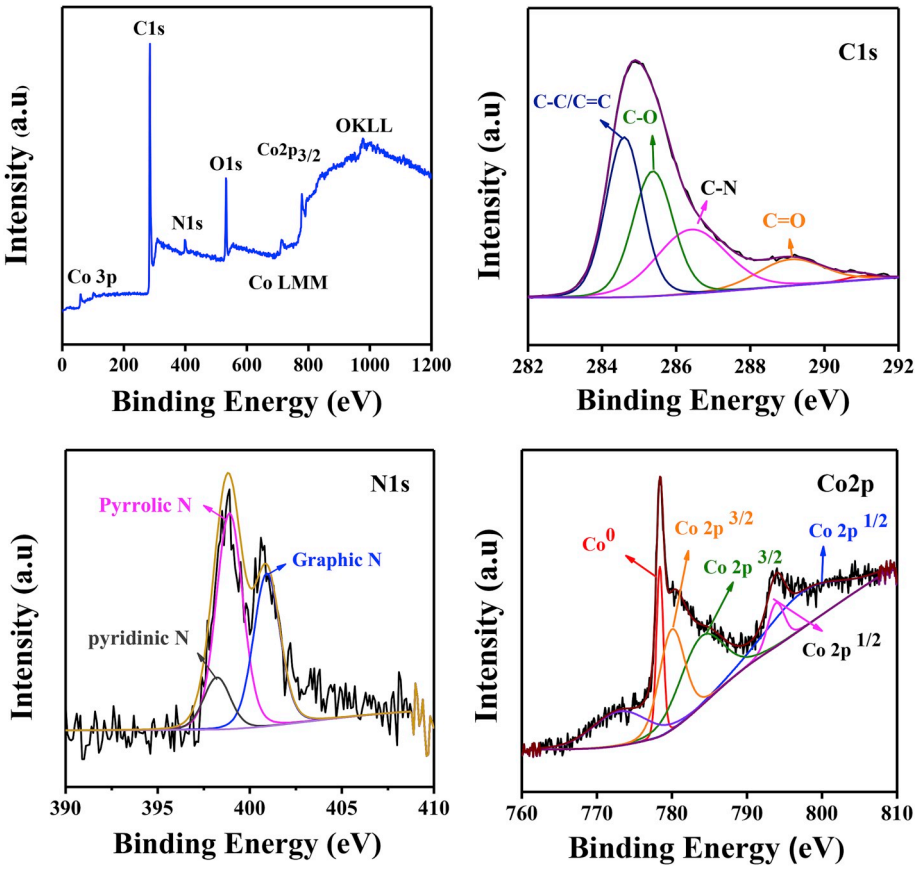

Fig. 4. XPS spectra of the representative prismatic Co/C nanocomposite (Co/C-650), (a) survey spectrum, (b) C1s spectrum, (c) Co2p spectrum and (d) N1s spectrum.

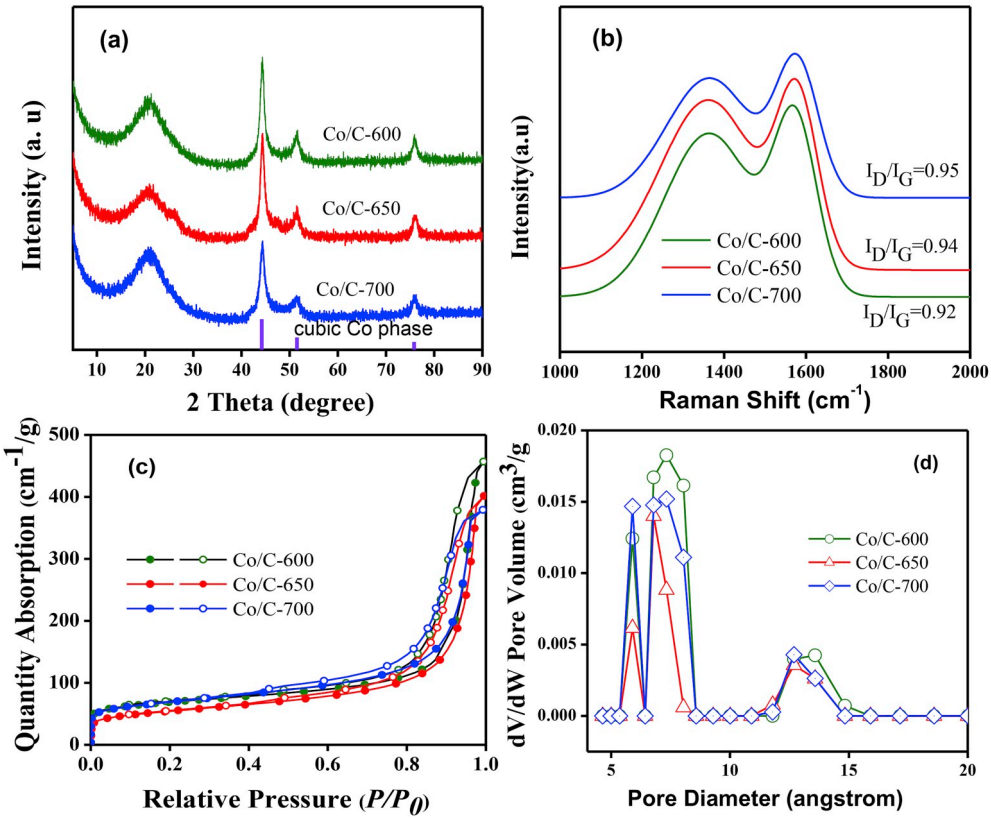

Fig. 5. XRD patterns where Cubic Co phase is according to JCPDS # 15–0806 (a), Raman spectra (b), nitrogen adsorption-desorption isotherm (c) and pore diameter distribution (d) of the prismatic Co/C nanocomposites.

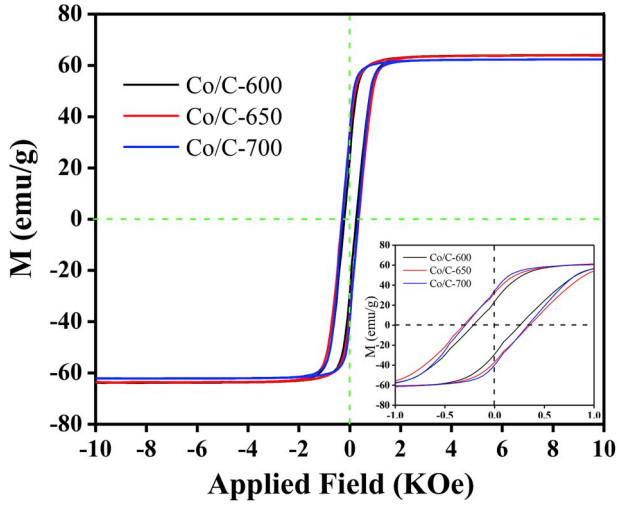

Fig. 6. Magnetic hysteresis loops of the prismatic Co/C nanocomposites, the insert image is corresponding with magnetic loops at low applied magnetic field.

2.3. Preparation of prismatic Co/C nanocomposites

The as-synthesized [$Co(INA)_2$] was placed in a tubular furnace under argon atmosphere for pyrolysis at 2 h with a heating rate of 2 °C/min. The pyrolysis temperature was set as 600 °C, 650 °C and 700 °C, respectively. The obtained Co/C nanocomposite sample was denoted as Co/C-600, Co/C-650 and Co/C-700 according to the pyrolysis temperature, respectively.

2.4. Characterization and measurements

The powder X-ray diffraction data of [$Co(INA)_2$] crystals were tested by X ray diffractometer (XRD), the model is Rigaku Mini Flex 600) and using Cu Kα. The morphologies of the materials were observed by high resolution scanning electron microscope (SEM Verios G4) and high resolution transmission electron microscope (TEM) with Talos F200X. Composition of elements were tested on X-ray photoelectron spectroscopy (XPS) with the model Kratos Axis Ultra DLD (Al Kα radiation generated at 15 kV and 150 W). Thermogravimetry (TG) curves of were recorded on STA 449 F3 under argon in the temperature 40–1000 °C under argon atmosphere. Raman spectra were measured on Renishaw via Raman microscope with an argon laser with an excitation of 532 nm, the spot size is 2 mm. Magnetic properties of samples was measured by vibrating sample magnetometer (VSM) at room temperature, the model is Lake Shore 7307. Nitrogen adsorption-desorption isotherms were measured according to Brunauer–Emmett–Teller (BET) method with 3 Flex model, Pyrolyzed samples need to be activated at 100 °C to remove solvents and water molecules before measurement. The electromagnetic parameters of the prismatic Co/C nanocomposites were tested on a vector network analyzer (VNA, MS4644A, Anritsu, Atsugi, Japan) in the 2–18 GHz range. The as prepared Co/C nanocomposites were well-dispersed in the paraffin matrix with 33% mass score. The coaxial ring with the outer diameter of 7.0 mm and inter diameter of 3.04 mm was made under the pressure of the tablet press.

3. Results and discussion

The synthesis strategy of [$Co(INA)_2$] MOF is shown in Fig. 1. The Co^{2+} was reacted with isonicotinic acid ligand to form the cubic [$Co(INA)_2$] MOF. Subsequently, the cubic MOF was pyrolyzed in argon atmosphere to generate the prismatic Co/C nanocomposites. As illustrated

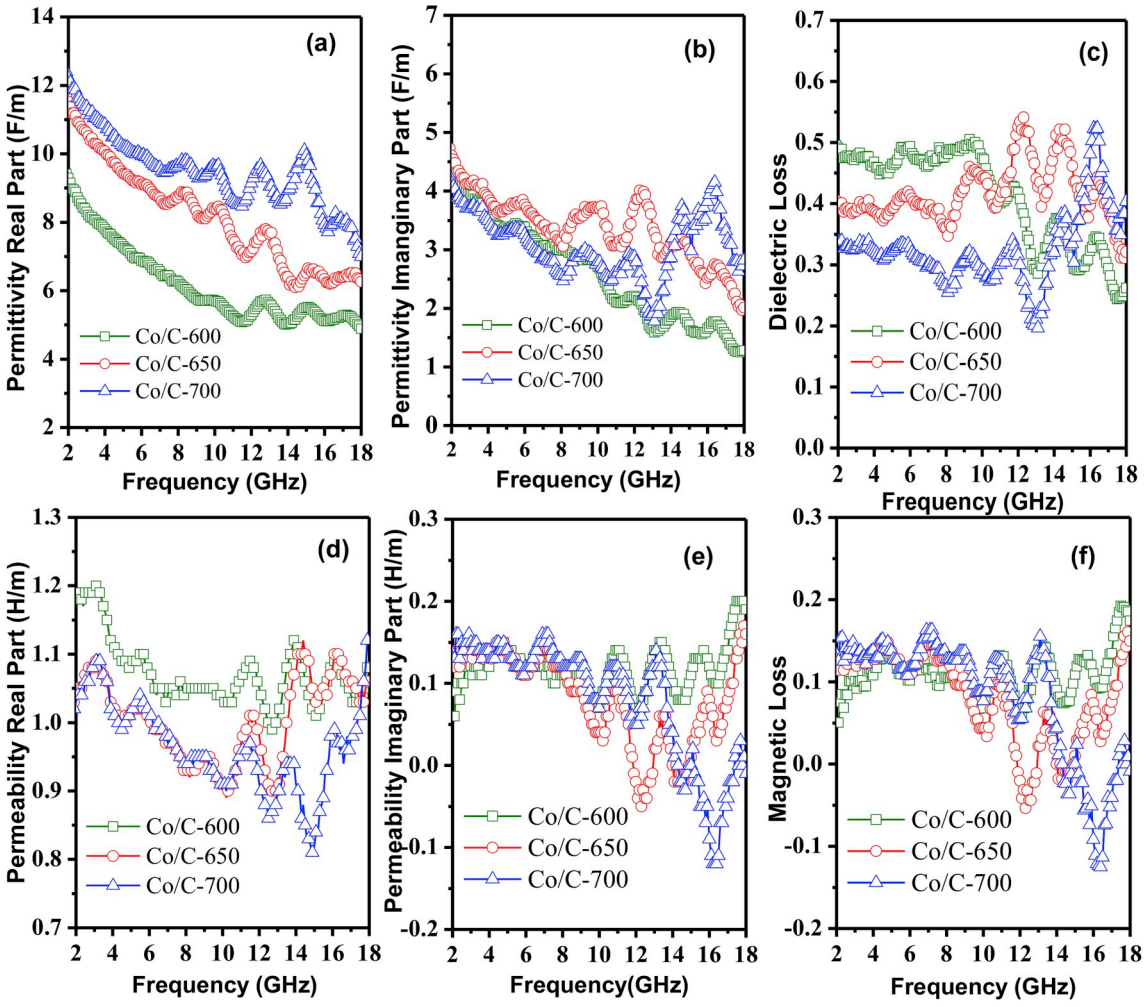

Fig. 7. Real part, imaginary parts and dielectric loss of complex permittivity (a, b, c) and real part, imaginary parts and dielectric loss of complex permeability (d, e, f) vs frequency for the prismatic Co/C nanocomposites.

in Fig. 2a, the characteristic diffraction peaks in XRD pattern can be well matched with the standard crystal data of $[Co(INA)_2]$ [25]. The two step weight loss of $[Co(INA)_2]$ was displayed in the TGA curve (Fig. 2b). The first stage around 160 °C is due to the removal of residual solvents and ligands and the weight sharply decreasing at 380 °C represents the gas evolution of organic groups and collapse of skeleton of ligand until the residual mass is unchanged above 600 °C.

The regular cubic structure of $[Co(INA)_2]$ MOF can be obviously observed as shown in Fig. 3a. The size is in micrometer scale (about 10 μm) and some debrises on surface are caused by ultrasonication in alcohol. After pyrolysis at 600–700 °C in argon atmosphere, the prismatic Co/C nanocomposites can be obtained as shown in Fig. 3b. Due to the strong skeleton of $[Co(INA)_2]$, the morphology of MOF was not destroyed even at 600–700 °C and prismatic shape was well reserved for Co/C nanocomposites. The TEM image of representative Co/C-650 in Fig. 3c demonstrates that numerous cobalt nanoparticles are embedded in the carbon layers. In the high-resolution magnification TEM image (Fig. 3d), the lattice fingers with d-spacing 0.20 nm is corresponding with (111) plane of cobalt crystals and the lattice fingers with d-spacing 0.34 nm is attributed to graphitic carbons. It indicates that the pyrolysis in argon atmosphere induces in situ formation of cobalt nanoparticles and graphitic carbons from $[Co(INA)_2]$ MOF.

In order to analyze atom valence state and element composition of prismatic Co/C nanocomposite, their XPS patterns are presented in Fig. 4. The existence of elements of C, N, O and Co was proved. The C1s peak in Fig. 4b is divided into four peaks, which is correspond to C–C/C═C (284.6 eV), C–O (285.9 eV), C–N (286.5eV) and C═O (289.2eV), respectively [26]. To verify the cobalt atom valence state in Co/C-650 (Fig. 4c), the deconvolution of Co2p peak indicates three valence states, i.e. Co^0 atoms (778.3 eV) Co^{3+} ions (780.9 eV and 786.5 eV) and Co^{2+} ions (796.8 eV and 803.4 eV) [27]. The oxidized species of cobalts are due to the surface oxidization in air or oxidization during pyrolysis. The XPS spectrum of nitrogen from nitrogen heterocyclics in isonicotinic acid ligand is shown in Fig. 4c, where the pyridinic nitrogen at 398.3 eV, pyrolytic nitrogen at 400.3 eV and graphitic nitrogen at 401.5 eV are presented.

The phase structure of Co/C nanocomposites can be verified from their XRD patterns presented in Fig. 5a. The strong diffraction peaks at $2\theta = 44.2°$, 51.5° and 75.9° are in agreement with (111), (200) and (220) planes, respectively, which fits well with the PDF card No. 15–0806. It proves the face-centered cubic structure of cobalts. Furthermore, the intensity of Co diffraction peaks becomes stronger when the temperature is raised. It demonstrates that the crystallinity of cobalt is enhanced. In addition, all the samples show an obvious diffraction peak around 20°. It indicates the formation of graphitized carbons during pyrolysis. The detailed chemical speciation of carbons was measured by Raman spectroscopy. In Fig. 5b, all the samples show two obvious peaks at D band (1340 cm^{-1}) and G band (1580 cm^{-1}), where D band represents disordered carbon or defective graphitic while G band represents some ordered carbon [28]. In general, the ratio of I_D/I_G is a usual criterion to judge the graphitic degree of carbons [9]. In this case, the I_D/I_G value of Co/C-600, Co/C-650 and Co/C-700 is 0.92,

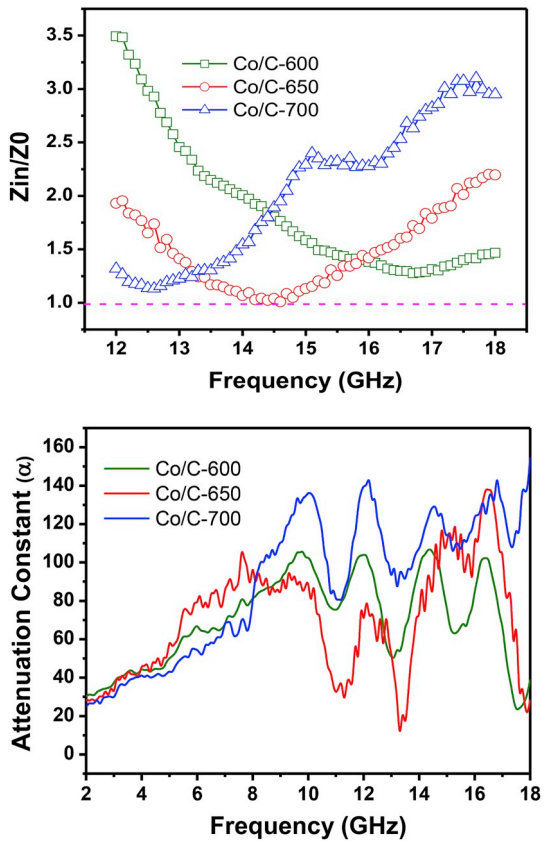

Fig. 8. Z_{in}/Z_0 values in the thickness of 2.0 mm (a) and attenuation constant (b) of prismatic Co/C nanocomposites (Co/C-600, Co/C-650 and Co/C-700).

0.94 and 0.95, respectively. It illustrates that more defective and disordered carbon are formed with the increased pyrolysis temperature.

The N_2 sorption experiment was carried out at 77 K to characterize the porosity and surface area of prismatic Co/C nanocomposites. The hysteresis loops can be obviously seen at high relative pressure in Fig. 5c, which demonstrates the existence of mesopores. Accordingly, a lower uptake below 0.1 P/P_0 represents tiny micro porosity. In this case, the Brunauer-Emmet-Teller (BET) surface is 237 m^2/g for Co/C-600, 183 m^2/g for Co/C-650 and 230 m^2/g for Co/C-700, respectively. The discrete fourier transformation (DFT) pore size analysis results are showed in Fig. 5d, where three remarkable pore size distribution regions (5 Å, 7 Å and 12 Å) can be found. It is caused by the collapse of MOF and carbon reorganization during pyrolysis process. It should be pointed out that the large surfaces areas and plentiful micropores in material are favorable for the attenuation of EM wave. The magnetic response of cobalt in prismatic Co/C nanocomposites was characterized using vibration magnetometer. Fig. 6 exhibits a typical ferromagnetic hysteresis loop for the three samples. The saturation magnetization (M_s) value for Co/C-600, Co/C-650 and Co/C-700 is 23.3 emu/g, 32.1 emu/g and 35.0 emu/g, respectively. The high saturation magnetization and Curie temperature of metallic cobalt are beneficial for the domain vibration under the action of external magnetic field [29]. The coercivity (H_c) of Co/C-600, Co/C-650 and Co/C-700 is 257 Oe, 363 Oe and 345 Oe, respectively. The value of H_c is associated with the grain size of magnetic cobalt. The H_c will increase at first and decrease from the peak value with increase of grain size (within the particle meter of 70 nm).

In general, the EM wave absorption in media is mainly related to complex permittivity (ε_r) and complex permeability (μ_r). The complex permittivity includes the real part (ε') and imaginary part (ε''), where the ε' represents storage of EM energy and the ε'' represents dissipation of EM energy, The complex permeability contains real part (μ') and imaginary part (μ'') related to magnetic storage capacity and magnetic loss, respectively [30,31]. The tangent of dielectric loss ($tan\delta_\varepsilon = \varepsilon''/\varepsilon'$) illuminates the dielectric loss ability while the magnetic loss tangents ($tan\delta_\mu$) shows the magnetic loss ability. From Fig. 7a–b, the ε' of prismatic Co/C nanocomposites decrease when the frequency is increased. The ε' of Co/C-700 is higher than those of Co/C-600 and Co/C-650. The ε'' with several obvious resonant peaks decreases from 4.5 to 1.0 in 6–16 GHz. It is caused by dielectric polarization, including dipolar polarization and interface polarization. The dipolar polarization is caused by porous carbon and interface polarization is induced by the air-Co/C interface and Co–C interface [32,33]. The attenuation constant (α) is shown in Fig. 8. The α of Co/C-700 is higher than those of other two samples between 8 and 18 GHz. However, the Co/C-700 does not show the best EM wave absorbing performance because of the impedance mismatch. The μ' and μ'' in Fig. 7d–e also showed some resonant peaks. It is due to polarization relaxation, resonance exchange, eddy current effect and natural ferromagnetic resonance in the frequency of 12–18 GHz. As a result, the $tan\delta\varepsilon$ and $tan\delta\mu$ are exhibited in Fig. 7c and f. Here, the $tan\delta_\mu$ is much lower than $tan\delta_\varepsilon$, which demonstrates that the dielectric loss plays the main role in microwave attenuation of the prismatic Co/C nanocomposites.

According to transmission line theory, the RC value can be calculated by the following formula [34].

$$RC\ (dB) = 20 \log \left| \frac{Z_{in} - 1}{Z_{in} + 1} \right| \quad (1)$$

$$Z_{in} = \sqrt{\frac{\mu_r}{\varepsilon_r}} \tanh \left[j \left(\frac{2\pi}{f} \right) fd \sqrt{\mu_r \varepsilon_r} \right] \quad (2)$$

where Z_{in} represents the impedance of absorber, μ_r is the relative complex permeability constant, ε_r represents the relative complex permittivity, f is the frequency in 2–18 GHz, d is the thickness of absorbers and c is the speed of light in vacuum condition. The RC value lower than −10 dB means that more than 90% electromagnetic wave can be absorbed.

The reflection coefficient of the prismatic Co/C nanocomposite was measured between 2 and 18 GHz. The minimum RC of Co/C-600 can reach −48.9 dB at a thickness of 3.1 mm and the EAB is 4.36 GHz (Fig. S1, Supporting Information). However, as shown in Fig. 9a, c, e, the Co/C-650 shows extraordinary absorption ability at a thickness of 2.0 mm, i.e. RC of −47.6 dB and EAB of 5.11 GHz. For Co/C-700 (Fig. 9b, d, f), the best absorption performance with the minimum RC of −45.4 dB occurs at a thickness of 2.5 mm. If the thickness of all samples is set as 2.0 mm, the EAB is 3.6 GHz (14.3–17.9 GHz) for Co/C-600, 5.1 GHz (12.1–17.2 GHz) for Co/C-650 and 4.6 GHz (11.6–16.2 GHz) for Co/C-700, respectively. As the thickness increases, the RC peak will shift to low frequency. The Co/C-650 exhibits the best EM wave absorption. To better explain the difference in absorption of samples, the value of Z_{in}/Z_0 can be considered. When the impedance of materials (Z_{in}) and the impedance of free space (Z_0) are almost equal, the value of Z_{in}/Z_0 is close to 1. It represents that most EM wave can enter the absorbers. Through the calculation by Eq. (2), the graph of Z_{in}/Z_0value is displayed in Fig. 8. The Co/C-650 is more near to 1 between the 12–18 GHz, demonstrating good impedance match in comparison to other samples. Here we list some typical EM wave absorption performance for Co/C composites reported in Table 1 [35–39]. It can be found that the Co/C-650 in this work possesses more favorable EM wave absorption abilities.

The illustration of hypothesized interfacial-driven EM wave attenuation in prismatic Co/C nanocomposites is shown in Fig. 10. From a macroscope viewpoint, EM wave will be reflected and attenuated multiple times between nanoparticles. The magnetic domain resonance occurring in cobalt nanoparticles and interfacial polarizations at air-Co/C interface and Co–C interface determine the absorption and attenuation of electromagnetic waves. Since the dielectric relaxation is the main factor to the difference of EM wave absorption among the three samples. The relationship of ε' and ε'' can be described as the following equation by Debye relaxation theory [40].

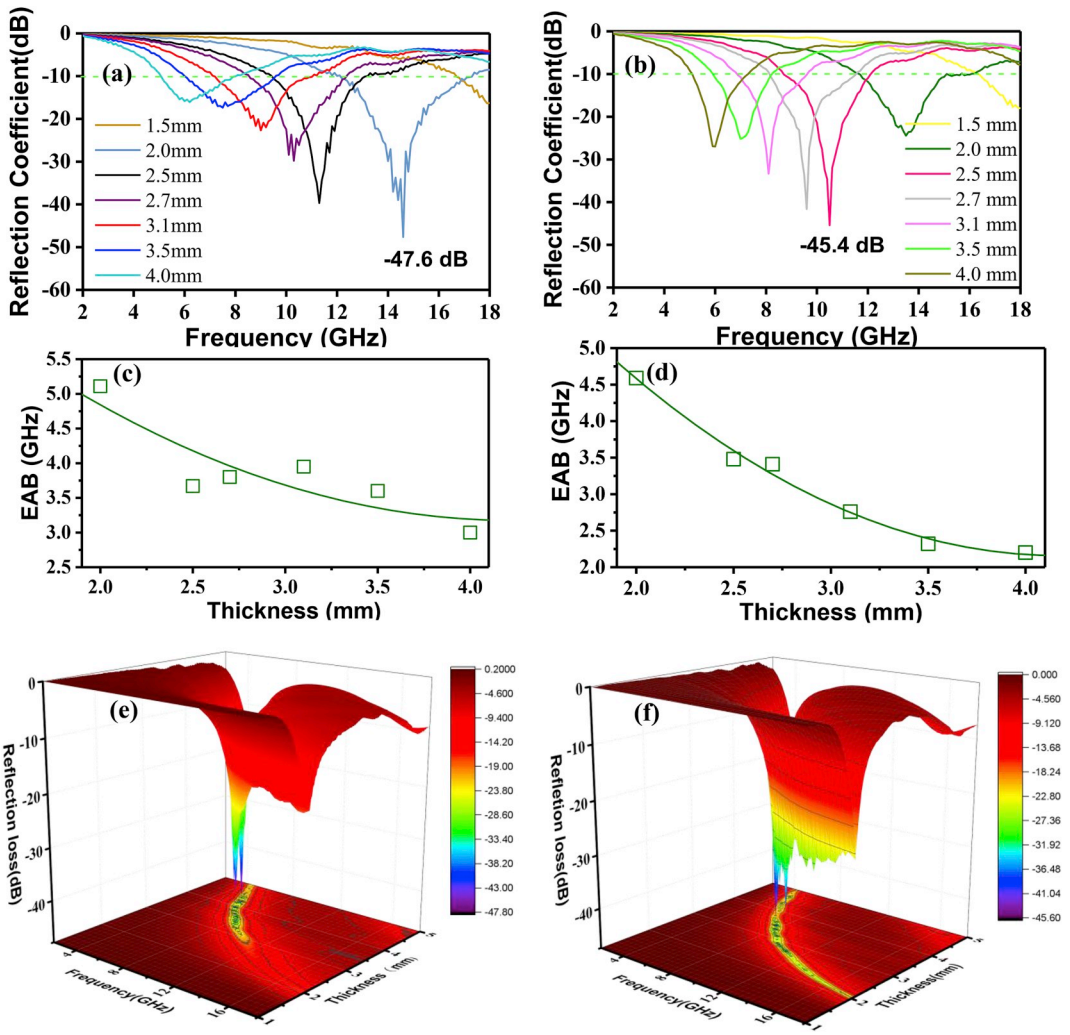

Fig. 9. Reflection coefficient (RC) (a, b), dependence of EAB with thickness (c, d) and 3D RC graphs of values of prismatic Co/C nanocomposites (Co/C-650 and Co/C-700).

Table 1
Comparison of reflection coefficient and effective absorption bandwidth of Co/C materials and similar Co/C nanocomposites.

Absorbers	Thickness (mm)	RC (dB)	EAB (GHz)	Ref.
Co/C-500	4.0	−35.3	2	[35]
Co/C-800	2.4	−62.12	5.0	[36]
Co@C microspheres	2.0	−30.2	3.0	[37]
Co/CNTs	1.8	−17.5	2.9	[38]
$Co_{2-x}P_x$/NC	1.5	−68	4.6	[39]
Co/C-650	2.0	−47.6	5.1	This work

$$\left(\varepsilon' - \frac{\varepsilon_s + \varepsilon_\infty}{2}\right)^2 + (\varepsilon'')^2 = \left(\frac{\varepsilon_s - \varepsilon_\infty}{2}\right)^2 \quad (3)$$

where ε_s is static permittivity, ε_∞ is relative permittivity in high frequency. The ε' and ε'' relationship deduced from the equation is generally regarded as Cole-Cole semicircle. Each semicircle demonstrates a Debye relaxation process. Fig. 11 and Fig. S2 show the plots of ε'-ε'' for the prismatic Co/C nanocomposites with Cole-Cole semicircles. The phenomenon is mainly caused by the two aspects. As the charge is accumulated at the interface under alternating EM field, the interfacial polarization at Co–C interface will be enhanced. On the other hand, as revealed in Fig. 5b, the carbons in nanocomposite possess lots of defects

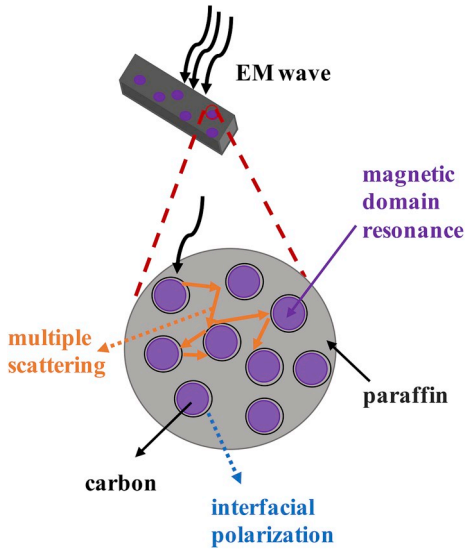

Fig. 10. The microwave absorption mechanisms of the Co/C composite derived from MOF precursor as a sacrifice template.

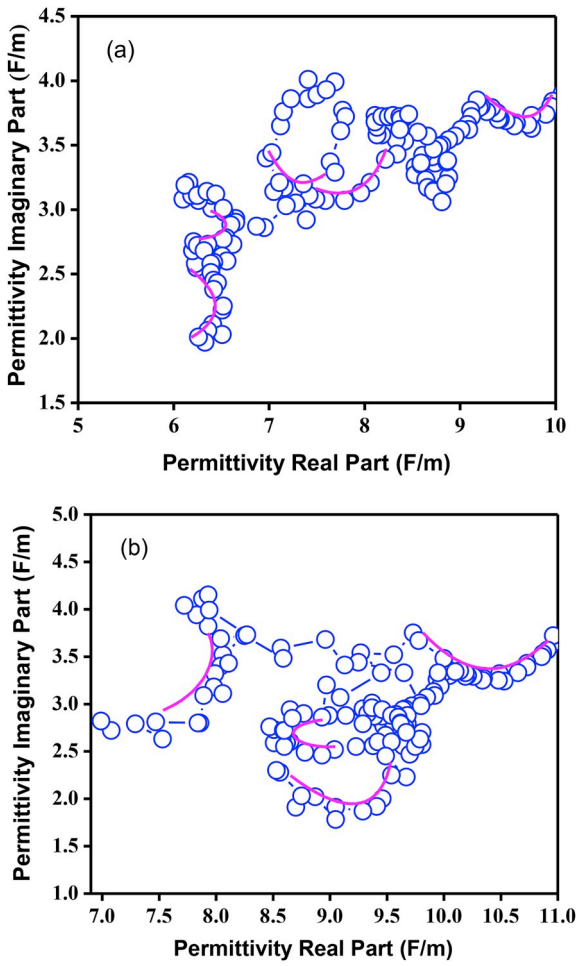

Fig. 11. Plots of ε′-ε′′ for prismatic Co/C nanocomposite of Co/C-650 (a) and Co/C-700 (b) in the frequency of 2–18 GHz.

including oxygen-containing chemical bonds on graphitic carbons, such as C═O and C–O bonds. They will become the polarization centers to produce dipole polarization. The multiple dipole and interfacial polarizations are in correspondence with the Cole−Cole semicircles and attenuate the EM wave. Thus the favorable EM wave absorption is achieved for the prismatic Co/C nanocomposites.

4. Conclusions

The cubic $[Co(INA)_2]$MOF was synthesized via an eco-friendly and convenient method by using cheap and non-toxic isonicotinic acid as organic ligand. After pyrolysis of $[Co(INA)_2]$ MOF at 600–700 °C, the Co/C nanocomposites could be well prepared with prismatic shapes and highly effective EM wave absorption ability. The pyrolysis temperature can affect their electromagnetic properties. The Co/C-650 pyrolyzed at 650 °C shows the best EM wave absorption ability. The minimum RC value can reach −47.6 dB and the EAB is 5.11 GHz at a thickness of 2.0 mm. If the thickness of all the samples is set as 2.0 mm, the EAB is 3.6 GHz (14.3–17.9 GHz) for Co/C-600, 5.1 GHz (12.1–17.2 GHz) for Co/C-650 and 4.6 GHz (11.6–16.2 GHz) for Co/C-700, respectively. Since the prismatic nanocomposites show favorable impedance matching and extraordinary EM wave absorption ability from C band to Ku band, they possess great potential in engineering application of electromagnetic wave absorbing/shielding devices and systems.

Declaration of competing interest

The authors declare that they have no known competing financial interests or personal relationships that could have appeared to influence the work reported in this paper.

Acknowledgments

This work was financially supported by the National Natural Science Foundation of China (21875190), the Natural Science Basic Research Plan in Shaanxi Province of China (2018JC-008, Distinguished Young Scholar), the Shaanxi Province Key Research and Development Plan for Industry Innovation Chain (Cluster) (2018ZDCXL-GY-09-07). K.C. thanks the National Young Talents Plan and Fundamental Research Funds for the Central Universities (3102017jc01001).

Appendix A. Supplementary data

Supplementary data to this article can be found online at https://doi.org/10.1016/j.compositesb.2019.107613.

Author statement

We are confident the novelty of the work and the results have not been published, in whole or in part, and is not under consideration in any other journal. The manuscript has been read and approved by all named authors.

References

[1] Kong L, Wang C, Yin X, Fan X, Wang W, Huang J. Electromagnetic wave absorption properties of a carbon nanotube modified by a tetrapyridinoporphyrazine interface layer. J Mater Chem C 2017;5(30):7479–88.
[2] Lan D, Qin M, Yang R, Chen S, Wu H, Fan Y, Fu Q, Zhang F. Facile synthesis of hierarchical chrysanthemum-like copper cobaltate-copper oxide composites for enhanced microwave absorption performance. J Colloid Interface Sci 2019;533:481–91.
[3] Singh S, Akhtar M, Kar K. Impact of Al_2O_3, TiO_2, ZnO and $BaTiO_3$ on the microwave absorption properties of exfoliated graphite/epoxy composites at X-band frequencies. Compos B Eng 2019;167:135–46.
[4] Rohini R, Bose S. Electrodeposited carbon fiber and epoxy based sandwich architectures suppress electromagnetic radiation by absorption. Compos B Eng 2019;161:578–85.
[5] Wang X, Yin L, Chen C, Yu J, Zhou X, Wang H, Xu B, Wei S. Synthesis of tremella-like graphene@SiC nano-structure for electromagnetic wave absorbing material application. J Alloy Comp 2018;741:205–10.
[6] Zhao B, Zhang X, Deng J, Bai Z, Liang L, Li Y, Zhang R. A novel sponge-like 2D Ni/derivative heterostructure to strengthen microwave absorption performance. Phys Chem Chem Phys 2018;20(45):28623–33.
[7] Sun X, Lv X, Li X, Yuan X, Li L, Gu G. Fe_3O_4@SiO_2 nanoparticles wrapped with polypyrrole (PPy) aerogel: a highly performance material as excellent electromagnetic absorber. Mater Lett 2018;221:93–6.
[8] Wang Y, Fu Y, Wu X, Zhang W, Wang Q, Li J. Synthesis of hierarchical core-shell $NiFe_2O_4$@MnO_2 composite microspheres decorated graphene nanosheet for enhanced microwave absorption performance. Ceram Int 2017;43(14):11367–75.
[9] Liang C, Song P, Ma A, Shi X, Gu H, Wang L, Qiu H, Kong J, Gu J. Highly oriented three-dimensional structures of Fe_3O_4 decorated CNTs/reduced graphene oxide foam/epoxy nanocomposites against electromagnetic pollution. Compos Sci Technol 2019;181:107683.
[10] Zhou X, Jia Z, Feng A, Wang X, Liu J, Zhang M, Cao H, Wu G. Synthesis of fish skin-derived 3D carbon foams with broadened bandwidth and excellent electromagnetic wave absorption performance. Carbon 2019;152:827–36.
[11] Zhou X, Zhang C, Zhang M, Feng A, Qu S, Zhang Y, Liu X, Jia Z, Wu G. Synthesis of Fe_3O_4/carbon foams composites with broadened bandwidth and excellent electromagnetic wave absorption performance. Compos Part A-Appl S 2019;127:105627.
[12] Feng A, Ma M, Jia Z, Zhang M, Wu G. Fabrication of $NiFe_2O_4$@carbon fiber coated with phytic acid-doped polyaniline composite and its application as an electromagnetic wave absorber. RSC Adv 2019;9(44):25932–41.
[13] Feng A, Wu G, Wang Y, Pan C. Synthesis, preparation and mechanical property of wood fiber-reinforced poly(vinyl chloride) composites. J Nanosci Nanotechnol 2017;17(6):3859–63.
[14] Wadhawan A, Garrett D, Perez J. Nanoparticle-assisted microwave absorption by single-wall carbon nanotubes. Appl Phys Lett 2003;83(13):2683–5.
[15] Song W, Cao M, Fan L, Lu M, Li Y, Wang C, Ju H. Highly ordered porous carbon/wax composites for effective electromagnetic attenuation and shielding. Carbon 2014;77:130–42.

[16] Wang Z, Yang M, Cheng Y, Liu J, Xiao B, Chen S, Huang J, Xie Q, Wu G, Wu H. Dielectric properties and thermal conductivity of epoxy composites using quantum-sized silver decorated core/shell structured alumina/polydopamine. Compos Part A-Appl S 2019;118:302–11.
[17] Bai X, Zhai Y, Zhang Y. Green approach to prepare graphene-based composites with high microwave absorption capacity. J Phys Chem C 2011;115(23):11673–7.
[18] Liang C, Qiu H, Han Y, Gu H, Song P, Wang L, Kong J, Cao D, Gu J. Superior electromagnetic interference shielding 3D graphene nanoplatelets/reduced graphene oxide foam/epoxy nanocomposites with high thermal conductivity. J Mater Chem C 2019;7(9):2725–33.
[19] Wang L, Chen L, Song P, Liang C, Lu Y, Qiu H, Zhang Y, Kong J, Gu J. Fabrication on the annealed Ti_3C_2Tx MXene/Epoxy nanocomposites for electromagnetic interference shielding application. Compos B Eng 2019;171:111–8.
[20] Qiang R, Du Y, Chen D, Ma W, Wang Y, Xu P, Ma J, Zhao H, Han X. Electromagnetic functionalized Co/C composites by in situ pyrolysis of metal-organic frameworks (ZIF-67). J Alloy Comp 2016;681:384–93.
[21] Liu L, Wang L, Li Q, Yu X, Shi X, Ding J, You W, Yang L, Zhang Y, Che R. High-performance microwave absorption of MOF-derived core-shell Co@N-doped carbon anchored on reduced graphene oxide. ChemNanoMat 2019;5(4):558–65.
[22] Shu R, Li W, Wu Y, Zhang J, Zhang G. Nitrogen-doped Co-C/MWCNTs nanocomposites derived from bimetallic metal-organic frameworks for electromagnetic wave absorption in the X-band. Chem Eng J 2019;362:513–24.
[23] Miao P, Cheng K, Li H, Gu J, Chen K, Wang S, Wang D, Liu TX, Xu BB, Kong J. Poly (dimethylsilylene)diacetylene-Guided ZIF-based heterostructures for full ku-band electromagnetic wave absorption. ACS Appl Mater Interfaces 2019;11(19): 17706–13.
[24] Zhu B, Miao P, Kong J, Zhang X, Wang G, Chen K. Co/C composite derived from a newly constructed metal-organic framework for effective microwave absorption. Cryst Growth Des 2019;19(3):1518–24.
[25] Wei Q, Nieuwenhuyzen M, Meunier F, Hardacre C, James S. Guest sorption and desorption in the metal-organic framework $[Co(INA)_2]$ (INA=isonicotinate)-evidence of intermediate phases during desorption. Dalton Trans 2004;12: 1807–11.
[26] Yang X, Fan S, Li Y, Guo Y, Li Y, Ruan K, Zhang S, Zhang J, Kong J, Gu J. Synchronously improved electromagnetic interference shielding and thermal conductivity for epoxy nanocomposites by constructing 3D copper nanowires/thermally annealed graphene aerogel framework. Compos Part A-Appl S 2020;128: 105670.
[27] Mohamadi M, Kowsari E, Haddadi A, Yousefzadeh M. Fabrication, characterization and electromagnetic wave absorption properties of covalently modified reduced graphene oxide based on dinuclear cobalt complex. Compos B Eng 2019;162: 569–79.
[28] Zhang Y, Wang L, Zhang J, Song P, Xiao Z, Liang C, Qiu H, Kong J, Gu J. Fabrication and investigation on the ultra-thin and flexible Ti_3C_2Tx/co-doped polyaniline electromagnetic interference shielding composite films. Compos Sci Technol 2019;183:107833.
[29] Wang A, Wang W, Long C, Li W, Guan J, Gu H, Xu G. Facile preparation, formation mechanism and microwave absorption properties of porous carbonyl iron flakes. J Mater Chem C 2014;2(19):3769–76.
[30] Dai X, Du Y, Yang J, Wang D, Gu J, Li Y, Wang S, Xu B, Kong J. Recoverable and self-healing electromagnetic wave absorbing Check tor nanocomposites. Compos Sci Technol 2019;174:27–32.
[31] Luo C, Jiao T, Gu J, Tang Y, Kong J. Graphene shield by SiBCN ceramic: a promising high-temperature electromagnetic wave-absorbing material with oxidation resistance. ACS Appl Mater Interfaces 2018;10(45):39307–18.
[32] Zhang X-J, Guo A-P, Wang G-S, Yin P-G. Recent progress in microwave absorption of nanomaterials: composition modulation, structural design, and their practical applications. IET Nanodielectrics 2019;2(1):2–10.
[33] Qu Y, Du Y, Fan G, Xin J, Liu Y, Xie P, You S, Zhang Z, Sun K, Fan R. Low-temperature sintering Graphene/$CaCu_3Ti_4O_{12}$ nanocomposites with tunable negative permittivity. J Alloy Comp 2019;771:699–710.
[34] Luo C, Tang Y, Jiao T, Kong J. High-temperature stable and metal-free electromagnetic wave-absorbing SiBCN ceramics derived from carbon-rich hyperbranched polyborosilazanes. ACS Appl Mater Interfaces 2018;10(33): 28051–61.
[35] Wang K, Chen Y, Tian R, Li H, Zhou Y, Duan H, Liu H. Porous Co-C core-shell nanocomposites derived from Co-MOF-74 with enhanced electromagnetic wave absorption performance. ACS Appl Mater Interfaces 2018;10(13):11333–42.
[36] Yin Y, Liu X, Wei X, Li Y, Nie X, Yu R, Shui J. Magnetically aligned Co-C/MWCNTs composite derived from MWCNT-interconnected zeolitic imidazolate frameworks for a lightweight and highly efficient electromagnetic wave absorber. ACS Appl Mater Interfaces 2017;9(36):30850–61.
[37] Ding D, Wang Y, Li X, Qiang R, Xu P, Chu W, Han X, Du Y. Rational design of core-shell Co@C microspheres for high-performance microwave absorption. Carbon 2017;111:722–32.
[38] Wu N, Lv H, Liu J, Liu Y, Wang S, Liu W. Improved electromagnetic wave absorption of Co nanoparticles decorated carbon nanotubes derived from synergistic magnetic and dielectric losses. Phys Chem Chem Phys 2016;18(46): 31542–50.
[39] Liu T, Xie X, Pang Y, Kobayashi S. Co/C nanoparticles with low graphitization degree: a high performance microwave-absorbing material. J Mater Chem C 2016; 4:1727–35.
[40] Abdalla I, Yu J, Li Z, Ding B. Nanofibrous membrane constructed magnetic materials for high-efficiency electromagnetic wave absorption. Compos B Eng 2018;155:397–404.